Polyhedron 203 (2021) 115224

Contents lists available at ScienceDirect

Polyhedron

journal homepage: www.elsevier.com/locate/poly

Electron paramagnetic spectrum of dimanganic human serum transferrin

Molly M. Lockart, Kyle C. Edwards, John B. Vincent *, Brad S. Pierce *

Department of Chemistry, The University of Alabama, Tuscaloosa, AL 35487-0336, USA

ARTICLE INFO

Article history:
Received 26 February 2021
Accepted 13 April 2021
Available online 18 April 2021

Keywords:
Manganese
Transferrin
Electron paramagnetic resonance

ABSTRACT

An EPR signal for Mn(III) bound to the metal transport protein transferrin has been detected for the first time. The temperature dependence and simulations of the EPR signal are consistent with the Mn(III) centers being six-coordinate in an elongated tetragonal environment. Thus, the incorporation of Mn(III) within the Tf active site does not vastly alter the coordination number or active site geometry relative to native $Fe(III)_2$-Tf. This parallel mode EPR signal for $Mn(III)_2$-Tf could prove valuable for future studies aimed at determining the physiological relevance of $Mn(III)_2$-Tf.

1. Introduction

Manganese is an essential trace element for mammals; however, excess manganese is toxic to the neurological system. Numerous systems exist for Mn transport, probably leading to appreciable redundancy. Mn can be transported as Mn^{2+}, Mn(II)-citrate complexes, Mn(III)-transferrin (Tf), and possibly other forms. Tf is an approximately 80 kDa protein that is primarily responsible for the transport of Fe as Fe(III) from the bloodstream to the tissues. Tf is comprised of two lobes with approximately 40% sequence homology and nearly superimposable three-dimensional structures. As shown in Fig. 1, each lobe possesses a metal ion-binding site separated by ~43 Å in the closed metal-bound form; these metal-binding sites are designated N and C based on their proximity to each protein terminus. Each metal ion binds concomitantly with a synergistic anion, usually (bi)carbonate. Tf is selective for Fe(III) in a biological environment as its two metal sites are adapted to bind ions with large charge-to-size ratios. In the bloodstream the protein is only ~30% loaded with Fe(III), giving it the ability to coordinate other metal ions such as Mn(III). Consequently, Mn(III)-Tf could play a physiological role in Mn transport, although the significance, if any, of this transport is poorly understood and appears to be limited [1–3]. The importance of manganese transport by transferrin in healthy individuals has not been established. Because of the toxic effects of Mn bioaccumulation, most research on Mn-transferrin has focused on Mn transport across the blood–brain barrier or Mn incorporation into neural cells (for example, Refs. [4–28]). The significance of Tf in transport of manganese across the blood–brain barrier is still under investigation.

Serum apotransferrin (apoTf) binds two equivalents of Mn, one in each of the protein's two metal-binding sites in separate lobes of the protein, and the complex possesses an intense visible absorption band with a maximum at ~429 nm with an extinction coefficient of ~9×10^3 M^{-1} cm^{-1}, giving Mn_2-Tf a distinct brown color [28–32]. The presence of the visible charge transfer band suggested Mn was binding as the trivalent ion. Additional spectroscopic and magnetic studies of $Mn(III)_2$-Tf revealed that the protein bound the two Mn ions concurrent with 0.93 (bi)carbonate per Mn [31]. The $Mn(III)_2$-Tf had no EPR signal (in the conventional perpendicular mode) at 4.2 K, while static magnetic susceptibility measurements were consistent with the presence of two S = 2 centers, confirming that Mn^{3+} was the form bound [31]. $Mn(III)_2$-Tf had ultraviolet/visible maxima at 295, 330, and 430 nm. The development of the intense brown color did not require the addition of hydrogen peroxide and was significantly slower under anaerobic conditions, suggesting air oxidation of Mn(II) to Mn(III) [31]. Slow oxidation of coordinated Mn(II) to Mn(III) has been confirmed by X-ray absorption spectroscopy [33].

The binding of Fe to Tf prevents the binding of Mn, indicating that Mn(III) does not bind as tightly as Fe(III) [34]. This suggests that Mn(III) binds in the two Fe(III)-binding sites, comprised of two tyrosinate, one aspartate, and one histidine residue from the

Abbreviations: Tf, transferrin; apoTf, apotransferrin; CW, continuous wave.

* Corresponding authors at: Department of Chemistry and Biochemistry, 250 Hackberry Lane, Box 870336, The University of Alabama, Tuscaloosa, AL 35487-0336, USA.

E-mail addresses: jvincent@bama.ua.edu (J.B. Vincent), bspierce1@ua.edu (B.S. Pierce).

https://doi.org/10.1016/j.poly.2021.115224
0277-5387/

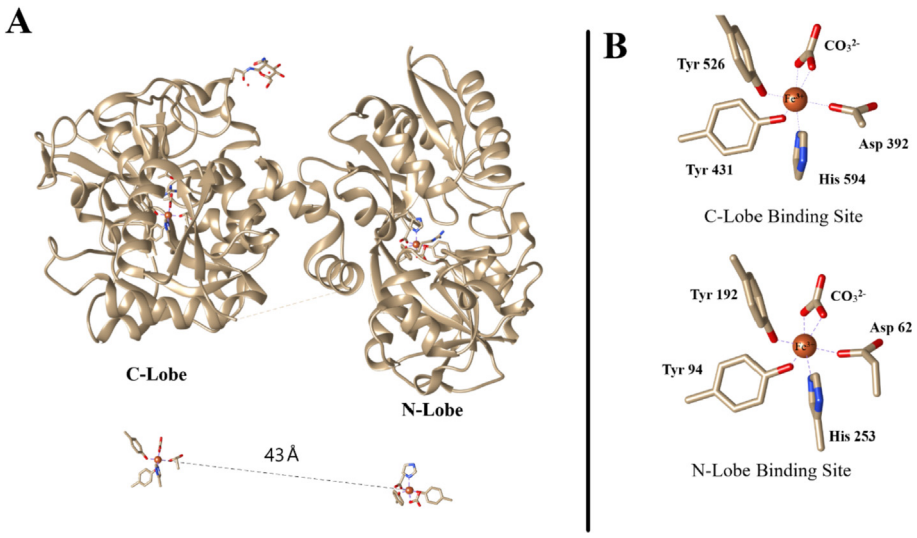

Fig. 1. A. X-ray crystallographic structure for porcine $Fe(III)_2$-Tf (pbd code 1H76) illustrating the distance separating the *N*-terminal from the C-terminal Fe-binding sites; no structure is yet available for the closed conformation of human $Fe(III)_2$-Tf. However, the porcine protein provided ligands are identical to those in the human protein. B. Comparison of the C-lobe and *N*-lobe metal binding sites of porcine $Fe(III)_2$-Tf.

protein and a bidentate synergistic ligand, normally (bi)carbonate. Resonance Raman spectra of $Mn(III)_2$-Tf suggest the binding of tyrosine to Mn(III) and the visible band arises from a phenoxide to Mn(III) charge transfer band [32]. Mn(III)-phenoxide complexes are generally not stable as the Mn(III) center normally oxidizes a bound phenoxide; the visible spectra of a synthetic Mn(III)-phenoxide compound (which appeared well after the biological study) appears to confirm the assignment of the visible band [35]. Excited energy transfer from a terbium ion bound in one site in transferrin to a ferric ion or manganic ion bound in the other metal-binding site indicates that the intersite distance is 3.55 ± 0.45 nm [36], again indicating that Mn(III) binds in the Fe(III) binding sites.

The binding of Mn^{2+} to serum apoTf as a function of the Mn:TF ratio has been followed by electronic and EPR spectroscopy [37]. The first equivalent of Mn^{2+} binds with $\log K_1$ = 4.06, while the second binds with $\log K_2$ = 2.96. Titration of mono-Fe(III)-Tf's (with Fe(III) selectively bound in either the C-terminal lobe or *N*-terminal lobe) with Mn^{2+} indicates that manganese can bind to either both Fe-binding site [37]. The titration gave $\log K_{C\text{-site}}$ = 3.80 and $\log K_{N\text{-lobe}}$ = 3.13. A mathematical model using the binding constants for Tf, albumin, and small molecules indicated that only a minor amount of Mn^{2+} should bind to transferrin in plasma, consistent with oxidation to Mn^{3+} being essential for tight binding of Mn to Tf [37]. Neither technique could monitor Mn(III) concentrations under the experimental conditions preventing binding constants for Mn(III) from being determined.

$Mn(III)_2$-Tf is capable of entering cells via endocytosis, similar to $Fe(III)_2$-Tf [33]. The addition of Mn to rat blood serum, goat blood serum, human blood serum, or bovine blood serum results in the binding of Mn to Tf [34,38–40]. Oral or intravenous administration of Mn^{2+} to rats results in Tf being the major Mn binding species in blood plasma [41]. $Mn(III)_2$-Tf competes with $Fe(III)_2$-transferrin for uptake into cells by Tf receptor [42].

Following the fate of $Mn(III)_2$-Tf *in vivo* or under biologically relevant conditions *in vitro* is difficult, particularly as no EPR signal has been previously reported. EPR spectroscopy has been shown to be a powerful method for studying the fates of Fe(III)-containing and Cr(III)-containing Tf [43–45]. As a metal center with an integral $S = 2$ spin, Mn(III) would be expected to give rise to an EPR signal in the parallel mode. The aim of the current work is to attempt to obtain a parallel mode EPR spectrum for $Mn(III)_2$-Tf, which could prove valuable for future studies aimed at determining the physiological relevance of $Mn(III)_2$-Tf.

2. Experimental

2.1. Materials

Iron-free human serum Tf was obtained from Aldrich (St. Louis, MO). Doubly deionized water was used throughout. All reagents were used as received unless otherwise notes. Mn(II) solutions were prepared using $MnCl_2{\cdot}4H_2O$ unless otherwise noted. ApoTf concentrations were determined by using the extinction coefficient ($\varepsilon = 9.12 \times 10^4\ M^{-1}\ cm^{-1}$) at 280 nm [46].

2.2. Preparation of $Mn(III)_2$-transferrin

Dimanganic-Tf was prepared using a variation of the literature procedure [31]. Human serum apo-Tf solution was dissolved in a 100 mM HEPES, 15 mM $NaHCO_3$ buffer at pH 7.4. An aliquot of Mn(II) solution was added to a solution of apo-Tf to give a Mn(II) to Tf ratio of 1.6:1, and the sample was stored at ~4 °C. The electronic spectrum of the solution was monitored over several days, and the concentration of Mn(III) bound to transferrin was determined using the extinction coefficient ($\varepsilon = 8.7 \times 10^3\ M^{-1}\ cm^{-1}$) at 427 nm [32]; after one week, all added Mn(II) was converted to Tf-bound Mn(III) within experimental error. Samples were frozen for EPR analysis with glycerol added to the solution (20/80 v/v).

2.3. Instrumentation

Ultraviolet–visible spectra were obtained using a Beckman Coulter (Brea, CA) DU800 UV–visible spectrophotometer.

2.4. EPR spectroscopy

Continuous wave (CW) EPR measurements were made on a Bruker (Billerica, MA) ELEXSYS E540 X-band spectrometer equipped with an ER 4116 dual mode resonator, an Oxford ESR900 cryostat, and an Oxford ITC 04 temperature controller for temperature-dependent measurements. Spectra were recorded in both parallel

and perpendicular mode at temperatures ranging from 4 to 60 K. Measurements used a nominal microwave frequency of 9.65 GHz and 9.41 GHz for microwave field polarization transverse and parallel to the applied magnetic field, respectively. Unless otherwise stated, all spectra were collected under non-saturating conditions with a modulation amplitude of 0.9 mT and a modulation frequency of 100 kHz.

2.5. Data analysis

CW EPR spectra were processed and simulated using SpinCount (version 6.4.7614.18037), which was developed by Professor Michael Hendrich at Carnegie Mellon University [47]. Parallel-mode Mn(III) (S = 2) spectra were simulated with the spin Hamiltonian,

$$\widehat{H} = \beta_e \vec{B}_0 \cdot \tilde{\boldsymbol{g}} \cdot \widehat{S} + \boldsymbol{D}\left(\widehat{S}_Z^2 - \frac{\widehat{S}^2}{3}\right) + \boldsymbol{E}\left(\widehat{S}_X^2 + \widehat{S}_Y^2\right) + \widehat{S} \cdot \tilde{\boldsymbol{A}} \cdot \widehat{I} \qquad (1)$$

where D and E describe the zero-field splitting terms, $\tilde{\boldsymbol{g}}$ is the g-tensor, and $\tilde{\boldsymbol{A}}$ is the nuclear hyperfine interaction, which is treated with second-order perturbation theory [48]. Simulations were calculated via diagonalization of Equation (1) and take into consideration all intensity factors, both theoretical and experimental. The concentration of species can be used as a constraint during spectral simulation, which allows quantitative determination of the concentration by comparison of the experimental and simulated signal intensities [47,49]. The only unknown factor relating the spin concentration to signal intensity is an instrumental factor that depends on the microwave detection system. This factor is determined using a Cu(II)EDTA spin standard [50].

3. Results and discussion

3.1. CW EPR spectroscopy

The perpendicular mode EPR spectra of $Mn(III)_2$-Tf (Fig. 2) exhibits a broad resonance near $g \sim 2.0$ with a sharp 6-line hyperfine splitting characteristic of hexaquaMn(II). At X-band (9 GHz), the microwave energy (hν-cm^{-1}) exceeds the axial zero field splitting for Mn(II) (typical D < 0.3 cm^{-1}), and thus signals for the d^5 ion (S = 5/2) are observed at $g \sim 2.0$ [47]. While the broadness of this signal suggests some heterogeneous or adventitious binding to the protein, the 9 mT hyperfine splitting (250 MHz) is diagnostic of ^{55}Mn(II) ($\boldsymbol{I}$ = 5/2). At first glance, the intensity of this signal suggests a significant concentration within the sample; however, as D < hν, transitions across all doublets are simultaneously observed, resulting in a significant enhancement in intensity. For perspective, relative to a S = 1/2 signal, the observed intensity from Mn(II) is increased by a factor of 35/3. Consequently, integration of the Mn(II) signal corresponds to <40 μM in the sample (~6% of the total Mn present in solution). An additional signal is observed at $g \sim 4.3$ in the perpendicular mode spectra. This signal originates from Fe $(III)_2$-Tf and accounts for ~20 αM (<6% of the total protein concentration) [51].

By altering the microwave field polarization parallel to the applied field, a new signal observed at $g \sim 8.3$ can be observed, which also exhibits a 6-line hyperfine splitting characteristic of ^{55}Mn (I = 5/2). Observation of this signal in parallel mode indicates that it originates from a "non-Kramers" doublet with an integer-spin. To first order, the effective g-value (g_{eff}) for a transition within a specific integer spin doublet is approximately four times the difference in m_s eigenstates [$g_{eff} = 4 \cdot \triangle m_s$] [47]. For instance, transitions within a | ±1 >, | ±2 >, and | ±3 > doublets are expected near $g \sim 4$, 8, and 12, respectively. Thus, the observed signal at $g \sim 8.3$ in parallel mode is consistent with a transition within an

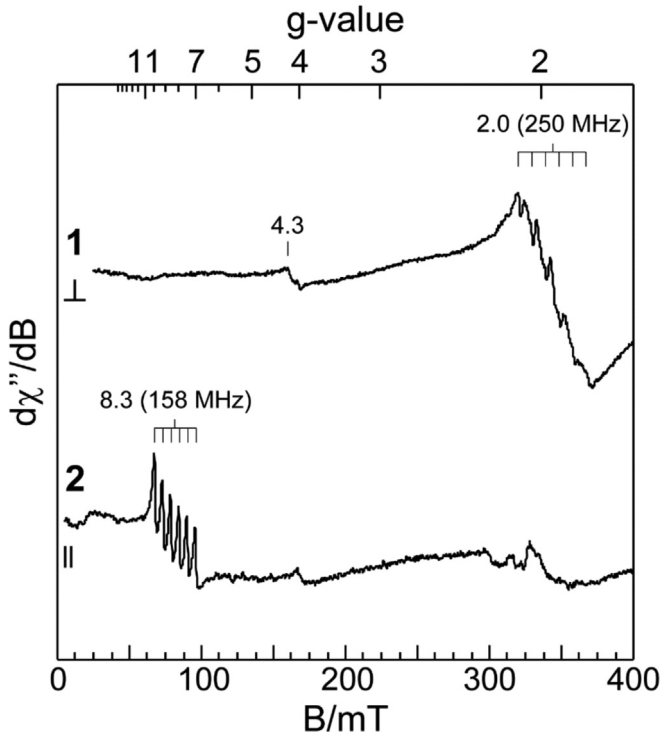

Fig. 2. Perpendicular and parallel mode X-band (9 GHz) CW EPR spectra of 0.38 mM $Mn(III)_2$-Tf. Instrumental parameters: microwave frequency, 9.64 GHz (perpendicular) and 9.41 GHz (parallel); microwave power, 20 mW; modulation amplitude, 0.9 mT; temperature, 15 K.

S = 2 spin manifold. Moreover, unlike the Mn(II) signal observed in perpendicular mode, the hyperfine splitting observed at $g \sim 8.3$ is separated by 5.9 mT (158 MHz). Thus, this feature cannot be attributed to Mn(II). Instead, this hyperfine splitting is consistent with values reported for Mn(III)-bound enzymes [52–56].

This Mn(III) must be bound in the two specific metal-binding sites in Tf. The ultraviolet/visible spectrum of $Mn(III)_2$-Tf prepared in the current study corresponds to those previously reported for $Mn(III)_2$-Tf. The change in the intensity of the absorbance at 427 nm in the visible spectrum observed during the formation of the $Mn(III)_2$-Tf corresponded within experimental error to that previously reported for $Mn(III)_2$-Tf [32]. This band has been shown to correspond to a tyrosine phenoxide to Mn(III) charge transfer band [32], consistent with Mn(III) binding to the two tyrosine residues in the metal-binding sites. The appearance of the charge transfer band has been found to be accompanied by the binding of 1 equivalent of (bi)carbonate per metal binding site [31], clearly requiring the Mn(III) to be bound in thespecific metal-binding sites.

The magnitude of the axial-zero field splitting term (D = −5 ± 1 cm^{-1}) for the Mn(III) was determined by fitting the temperature normalized $g \sim 8.3$ signal observed in parallel mode EPR to a theoretical Boltzmann population distribution for a S = 2 spin system (Equation (2)). The observed decreases in signal intensity with increasing temperature is consistent with a transition within the ground | ± 2 > doublet (between levels 1 and 2 as illustrated in Fig. 3).

$$Intensity \times T\ n_s = \frac{g_i e^{-\Delta E_i/k_b T}}{\sum_j g_j \cdot e^{-\Delta E_j/k_b T}} = \frac{(2S_i + 1) \cdot e^{-DS_{z,i}^2/k_b T}}{\sum_j (2S_j + 1) \cdot e^{-DS_{z,j}^2/k_b T}} \qquad (2)$$

Additional corroboration of the axial zero-field splitting term was obtained by simultaneous simulation of EPR spectra collected at temperatures ranging from 4 to 45 K. Within this temperature

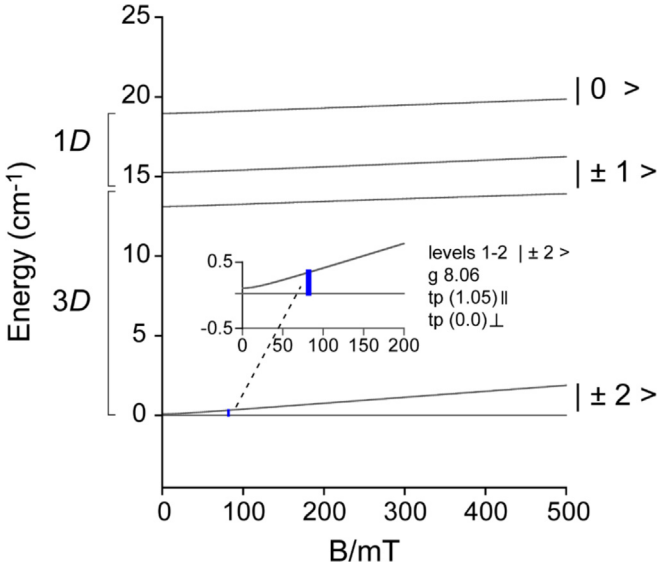

Fig. 3. Energy level diagram illustrating the splitting of doublets within the Mn(III) $S = 2$ spin system. For clarity, only the splitting along the z-principle axis is shown. The observed transition within the ground, | ± 2 > doublet is highlighted and transition probabilities (tp) are shown for both transverse and parallel field polarizations. The energy level was calculated using the same zero field splitting parameters and g-values identified by simulation of the $Mn(III)_2$-Tf EPR spectra (Shown in Fig. 3). [$S = 2$; $D = -5.0$ cm^{-1}; E/D, 0.08; $g_{1,2,3}$ (2.01, 2.01, 2.02)].

regime, all simulations accurately reproduce the relative intensity of the multiline g ~ 8.3 feature using a D-value of -4.7 ± 0.5 cm^{-1}. Within error, this is equivalent to the value obtained from fitting the temperature-dependent signal intensity to a Boltzmann distribution function. The magnitude of the D-value observed here is well within the range (1–5 cm^{-1}) typically reported for Mn(III) d^4-ions [52,54–56,57–60].

As shown in Fig. 4, the $Mn(III)_2$-Tf spectrum can be simulated (*dashed line*) using the measured D-value ($D = -4.7 \pm 0.5$ cm^{-1}) and a near axial rhombic contribution ($E/D = 0.08$) to the zero field

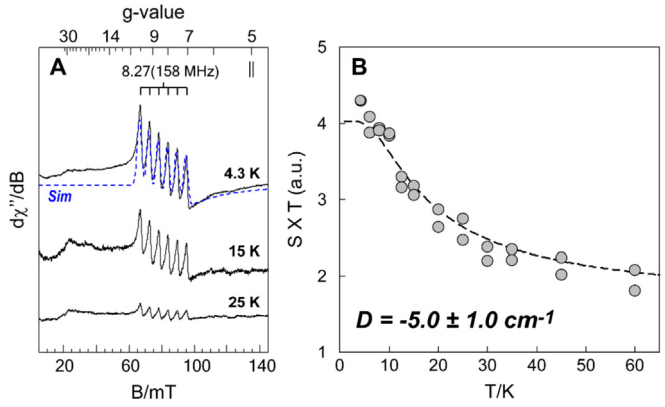

Fig. 4. A. Parallel mode CW-EPR spectra (*black traces*) of $Mn(III)_2$-Tf at selected temperatures (4.3, 15, and 25 K). The intensities of all spectra are normalized for temperature to correct for Curie Law. For comparison, quantitative EPR simulation (*dashed line*) is overlaid on the data. Instrumental parameters: microwave frequency, 9.41 GHz; microwave power, 21.12 mW; modulation amplitude, 0.9 mT. Simulation parameters: $S = 2$; $I = 5/2$ (100% abundance); $D = -5.0$ cm^{-1}; E/D, 0.08; $g_{1,2,3}$ (2.01, 2.01, 2.02); $\sigma_{E/D} = 0.007$; $A_{1,2,3}$(155, 155, 160) MHz; σ_B, 0.6 mT. B. Temperature normalized signal intensity (S × T) of the Mn(III) g ~ 8.3 resonance as a function of temperature. The axial zero field splitting ($D = -5.0 \pm 1.0$ cm^{-1}) for Mn (III) was modeled by fitting the temperature normalized data to a Boltzmann population distribution (*dashed line*) for a transition within the ground | ±2 > doublet of a $S = 2$ spin system.

splitting. Accordingly, g_z and A_z-values of the intrinsic g- and A-tensors were modeled as axial g_z (2.01) and A_z (158) MHz, respectively. The line width of the $S = 2$ site was largely dominated by distributions in E/D ($\sigma_{E/D} = 0.007$). While Fig. 4 only shows a simulation for 4.3 K spectrum, the intensity of the g ~ 8.3 signal is reproduced across all temperatures measured. Crucially, the Mn(III) concentration predicted from spectroscopic simulation accounts for 0.9 ± 0.2 mM, within experimental error of the concentration determined by electronic spectroscopy.

EPR spectroscopic simulations of the Mn(III)-sites are best fit to a single set of spectroscopic parameters (g-values, A-values, and zero field splitting terms). This suggests that the ligands and the coordination number at the Mn(III)-sites are uniform. Thus, Mn (III) bound in the two metal binding sites located in the N and C terminal domains of the protein cannot be differentiated by EPR. This has been observed previously for certain confirmations of Cr $(III)_2$-Tf [44].

4. Discussion

Among spectroscopically characterized Mn(III) complexes, the hyperfine splitting and axial zero field splitting are diagnostic of the coordination environment of the Mn(III) site [52–56]. For instance, the observed hyperfine splitting of $Mn(III)_2$-Tf (~158 MHz) is similar to values reported for 5- and 6-coordinate Mn-enzymes oxalate decarboxylase (OxDC) and manganese dependent superoxide dismutase (Mn-SOD) [61,62]. Of note, the 6-coordinate Mn(III)-site of OxDC also exhibits a negative axial zero field splitting ($D = -4.0$ cm^{-1}) [61]. In octahedral symmetry, the degeneracy of the ^{5}Eg state is removed by Jahn-Teller distortion resulting in either axial elongation ($D < 0$) or compression ($D > 0$) of the dz^2-orbital. In the case of axial elongation, the energy of the dz^2 orbital decreases relative to the dx^2-y^2 thus leaving the d^4 ion with an unoccupied dx^2-y^2 orbital [52,53]. The similarities in both hyperfine splitting and negative D-value, suggest that the Mn(III) sites in $Mn(III)_2$-Tf are very similar to that in OxDC in both coordination number and axial elongation. This suggests that the Mn(III) sites in $Mn(III)_2$-Tf pick up a synergistic ligand from solution and is consistent with $Mn(III)_2$-Tf being reported to possess 0.94 equivalents of (bi)carbonate per Mn(III) [31]. Therefore, incorporation of Mn(III) within the Tf active site does not vastly alter the coordination number or active site geometry relative to native Fe $(III)_2$-Tf.

5. Conclusion

Using CW EPR in the parallel mode, an EPR signal for the manganic centers in $Mn(III)_2$-Tf has been detected and characterized for the first time. Simulation of the signal and its temperature dependence reveal the hyperfine splitting and axial zero field splitting are diagnostic of the coordination environment of Mn(III). Consequently, the incorporation of Mn(III) within the Tf active site does not vastly alter the coordination number or active site geometry relative to native $Fe(III)_2$-Tf. As a result, parallel mode EPR signal for $Mn(III)_2$-Tf could prove valuable for future studies aimed at determining the physiological relevance of $Mn(III)_2$-Tf. A translational benefit of this work is demonstrating the utility of Tf as a robust protein scaffolding to provide spectroscopic (and potentially functional) models for Mn(III)-dependent enzymes such as oxalate decarboxylase and oxalate oxidase.

CRediT authorship contribution statement

Molly M. Lockart: Investigation, Writing - review & editing. **Kyle C. Edwards:** Investigation, Writing - review & editing. **John**

B. Vincent: Conceptualization, Writing - original draft, Writing - review & editing. **Brad S. Pierce:** Formal analysis, Writing - original draft.

Declaration of Competing Interest

The authors declare that they have no known competing financial interests or personal relationships that could have appeared to influence the work reported in this paper.

Acknowledgements

The authors wish to thank the editors for the invitation to submit to this special issue of *Polyhedron*. This work was supported by grants from the National Institutes of Health (2 R15 GM117511-01 to B.S.P.) and the National Institute of Science (CHE, 1709369 to B.S. P).

References

[1] G. Bjorklund, M. Dadr, M. Peana, M.S. Rahman, J. Aaseth, Arch. Toxicol. 94 (2020) 725–734.
[2] J.B. Vincent, S. Love, Biochim. Biophys. Acta 1820 (2012) 361–378.
[3] C. Herrera, M.A. Pettiglio, T.B. Bartnikas, J. Biol. Inorg. Chem. 19 (2014) 869–877.
[4] N. Suarez, E. Walum, H. Eriksson, Toxicol. In Vitro 9 (1995) 717–721.
[5] A.C.G. Chua, E.H. Morgan, J. Comp. Physiol. B 167 (1997) 361–369.
[6] A. Takeda, A. Devenyi, J.R. Connor J. Neurosci. Res. 51 (1998) 454-462.
[7] E.A. Malecki, A.G. Devenyi, J.L. Beard, J.R. Connor, Biometals 11 (1998) 265–276.
[8] E.A. Malecki, B.M. Cook, A.G. Devenyi, J.L. Beard, J.R. Connor, J. Neurol. Sci. 170 (1999) 112–118.
[9] A. Takeda, S. Ishiwatari, S., J. Neurosci. Res. 59 (2000) 542-552.
[10] E.A. Malecki, J. Nutr. 131 (2001) 1584.
[11] R.A. Yokel, Environ. Health Perspect. 110 (2002) 699–704.
[12] R.A. Yokel, J.S. Crossgrove, Res. Rep. Health Eff. Inst. 119 (2004) 7–58.
[13] J.S. Crossgrove, D.D. Allen, B.L. Bukaveckas, S.S. Rhineheimer, R.A. Yokel, Neurotoxicology 24 (2003) 3–13.
[14] J.S. Crossgrove, R.A. Yokel, Neurotoxicology 25 (2004) 451–456.
[15] G.J. Li, Q. Zhao, W. Zheng, Toxicol. Appl. Pharmacol. 205 (2005) 188–200.
[16] S.H. Reaney, D.R. Smith, Toxicol. Appl. Pharmacol. 205 (2005) 271–281.
[17] K.M. Erikson, M. Aschner, Neurotoxicology 27 (2006) 125–130.
[18] G.J. Li, B.-S. Choi, X. Wang, J. Liu, M.P. Waalkes, W. Zhang, Neurotoxicology 27 (2006) 737–744.
[19] S.J. Garcia, K. Gellein, T. Syversen, M. Aschner, Toxicol. Sci. 92 (2006) 516–525.
[20] S.H. Reamey, G. Bench, D.R. Smith, Toxicol. Sci. 93 (2006) 114–124.
[21] T.E. Gunter, C.E. Gavin, M. Aschner, K.K. Gunter, Neurotoxicology 27 (2006) 765–776.
[22] S.J. Garcia, K. Gellein, T. Syversen, M. Aschner, Toxicol. Sci. 95 (2007) 205–214.
[23] B. Michalke, A. Berthele, P. Mistriotis, M. Ochsenkuhn-Petropoulou, S. Halbach, J. Trace Elem. Med. Biol. 21 (S1) (2007) 4–9.
[24] X. Wang, D.S. Miller, W. Zheng, Toxicol. Appl. Pharmacol. 230 (2008) 167–174.
[25] V. Nischwitz, A. Berthele, B. Michalke, Anal. Chim. Acta 627 (2008) 258–269.
[26] X. Wang, G.J. Li, W. Zheng, Exp. Biol. Med. 233 (2008) 1561–1571.
[27] R.A. Yokel, Neuromol. Med. 11 (2009) 297–310.
[28] B.B. Williams, G.F. Kwakye, M. Wegrzynowicz, D. Li, M. Aschner, K.M. Erikson, A.B. Bowman, Toxicol. Sci. 117 (2010) 169–179.
[29] B.L. Vallee, D.D. Ulmer, Biochem. Biophys. Res. Commun. 8 (1962) 331–337.
[30] D.D. Ulmer, B.L. Vallee, Biochemistry 2 (1963) 1335–1340.
[31] P. Aisen, R. Aasa, A.G. Redfield, J. Biol. Chem. 244 (1969) 4628–4633.
[32] Y. Tomimatsu, S. Kint, J.R. Scherer, Biochemistry 15 (1976) 4918–4924.
[33] T.E. Gunter, B. Gerstner, K.K. Gunter, J. Malecki, R. Gelein, W.M. Valentine, M. Aschner, D.I. Yule, NeuroToxicology 34 (2013) 118–127.
[34] A.M. Scheuhammer, M.G. Cherian, Biochim. Biophys. Acta 840 (1985) 163–169.
[35] A.R. Schake, E.A. Schmitt, A.J. Conti, W.E. Streib, J.C. Huffman, D.N. Hendrickson, G. Christou, Inorg. Chem. 30 (1991) 3192–3199.
[36] P. O'Hara, S.M. Yeh, C.F. Meares, R. Bersohn, Biochemistry 20 (1981) 4704–4708.
[37] W.R. Harris, Y. Chen, J. Inorg. Biochem. 54 (1994) 1–19.
[38] R.C. Keefer, A.J. Barak, J.D. Boyett, Biochim. Biophys. Acta 221 (1970) 390–393.
[39] B. Panic, Acta Vet. Scand. 8 (1967) 228–233.
[40] R.A. Gibbons, S.N. Dixon, K. Hallis, A.M. Russell, B.F. Sansom, H.W. Symonds, Biochim. Biophys. Acta 444 (1976) 1–10.
[41] L. Davidsson, B. Lonnerdal, B. Sandstrom, C. Kunz, C.L. Keen, J. Nutr. 119 (1989) 1461–1464.
[42] D. Moutafchiev, L. Sirakov, P. Bontchev, Biol. Trace Elem. Res. 61 (1998) 181–191.
[43] K.C. Edwards, H.H. Kim, J.B. Vincent, J. Inorg. Biochem. 202 (2020) 110901.
[44] K.C. Edwards, H.H. Kim, R. Ferguson, M.M. Lockart, J.B. Vincent, J. Inorg. Biochem. 206 (2020) 111040.
[45] G. Deng, K. Wu, A. Cruce, M.K. Bowman, J.B. Vincent, J. Inorg. Biochem. 143 (2015) 48–55.
[46] J.M. Aramini, H.J. Vogels, J. Am. Chem. Soc. 115 (1993) 245–252.
[47] D.T. Petasis, M.P. Hendrich, Methods Enzymol. 583 (2015) 171–208.
[48] A. Abragam, B. Bleaney, Electron Paramagnetic Resonance of Transition Ions, Oxford University Press, Oxford, 2012.
[49] M.P. Hendrich, P.G. DeBrunner, Biophys. J. 56 (1989) 489–506.
[50] J.A. Weil, J.R. Bolton, J.E. Wertz, Electron Paramagnetic Resonance: Elementary Theory and Practical Applications, John Wiley & Sons Inc, New York, 1994.
[51] D.A. Folajtar, N.D. Chasteen, J. Am. Chem. Soc. 104 (1982) 5775–5780.
[52] L. Tao, T.A. Stich, A.V. Soldatova, B.M. Tebo, T.G. Spiro, W.H. Casey, R.D. Britt, J. Biol. Inorg. Chem. 23 (2018) 1093–1104.
[53] B.S. Pierce, M.P. Hendrich, J. Am. Chem. Soc. 127 (2005) 3613–3623.
[54] K.A. Campbell, D.A. Force, P.J. Nixon, F. Dole, B.A. Diner, R.D. Britt, J. Am. Chem. Soc. 122 (2000) 3754–3761.
[55] K.A. Campbell, E. Yikilmaz, C.V. Grant, W. Gregor, A.-F. Miller, R.D. Britt, J. Am. Chem. Soc. 121 (1999) 4714–4715.
[56] R. Gupta, T. Taguchi, A.S. Borovik, M.P. Hendrich, Inorg. Chem. 52 (2013) 12568–12575.
[57] M. Zheng, M.S.V. Khangulov, G.C. Dismukes, V.V. Barynin, Inorg. Chem. 33 (1994) 382–387.
[58] H.J. Gerritsen, E.S. Sabisky, Phys. Rev. 132 (1963) 1507–1512.
[59] J.M. Peloquin, K.A. Campbell, D.W. Randall, M.A. Evanchik, V.L. Pecoraro, W.H. Armstrong, R.D. Britt, J. Am. Chem. Soc. 122 (2000) 10926–10942.
[60] J. Krzystek, J. Telser, L.A. Pardi, D.P. Goldberg, B.M. Hoffman, L.-C. Brunel, Inorg. Chem. 38 (1999) 6121–6129.
[61] W. Zhu, J. Wilcoxen, R.D. Britt, N.G.J. Richards, Biochemistry 55 (2016) 429–434.
[62] Y. Sheng, T.A. Stich, K. Barnese, E.B. Gralla, D. Cascio, R.D. Britt, D.E. Cabelli, J.S. Valentine, J. Am. Chem. Soc. 133 (2011) 20878–20889.